

A CFD Investigation of Dragonfly Flight: Aerodynamic Analysis of Corrugated Wings Using Static and Dynamic Meshing in OpenFOAM

Gracye C. Lamb^{*}, Amirdhini C. Pechiammal[†], Aadhavan Magesh[‡], Devanshi Bhargava[§], Ananya Mahavratayajula[¶],
Jonah C. Holloway^{||}, and Alexander R. Miramontes^{**}
Exascale Computational Fluid Dynamics, Vertically Integrated Project
Georgia Institute of Technology, Atlanta, Georgia, 30332

For decades, researchers have attempted to synthesize the flight maneuverability of the dragonfly using various experimental methods. The biological and structural properties of dragonflies – particularly their highly corrugated wing pattern and agile flight mechanics – reveal desirable aerodynamic capabilities to reproduce, such as by micro-air vehicles, which have long been central to the discussion of related experimental applications. However, a particular challenge in replicating such flight characteristics appears as the specific stroke patterning of flexible dragonfly wings retain many degrees of freedom and have yet to be fully understood. Although studies exist on the flapping mechanics of rigid wing aerodynamics that yield solutions to the Navier-Stokes equations, many use highly simplified wing structures, proving insufficient to meet the objective of replicating dragonfly flight. Thus, we employ an investigation into the application of dynamic meshing and mesh refinement techniques using OpenFOAM to analyze 3D flight of fully reconstructed Odonata wings. By using a static meshing technique to simulate the fidelity of our method, we developed our dynamic meshing technique with the construction of an Arbitrary Mesh Interface, allowing control over key kinematic factors of our flight mechanics. The results of our simulations on an *Orthetrum caledonicum* forewing yield C_L and C_D values with fixed and variable angle of attack as well as respective flow visualization of the flapping motion. Further, this study serves as justification to extend dynamic meshing techniques to engage full control over dragonfly flapping patterns of greater complexity, if applicable, and bolster insights to modeling complex flight patterns of biological systems and advanced micro-air vehicles.

I. Nomenclature

A	=	amplitude of flapping oscillation
AR	=	Aspect Ratio
α	=	alpha, angle of attack
β	=	dihedral angle
C_D	=	drag coefficient
C_L	=	lift coefficient
dt	=	time step
Re	=	Reynolds number

^{*}Undergraduate, Aerospace Engineering, AIAA Student Member, 1537369

[†]Undergraduate, Aerospace Engineering, AIAA Student Member, 1760262

[‡]Undergraduate, Aerospace Engineering, AIAA Student Member, 1537191

[§]Undergraduate, Aerospace Engineering, AIAA Student Member, 1809833

[¶]Undergraduate, Aerospace Engineering, AIAA Student Member, 1596170

^{||}Undergraduate, Aerospace Engineering, AIAA Student Member, 1810796

^{**}Undergraduate, Mechanical Engineering, AIAA Student Member, 1760562

II. Introduction

DRAGONFLIES exhibit remarkable flight capabilities due to their unique corrugated wing structures that serve to enhance their flight performance. Their flight mechanics allow for precise control and heightened aerodynamic performance, generating complex flow structures that enhance lift and control airflow. The biological adaptations that dragonflies have make them ideal models for bio-inspired air vehicle design, particularly when it comes to micro-air vehicles (MAVs). MAVs are crucial for a variety of applications, including environmental monitoring, search and rescue operations, and military reconnaissance, where small, highly maneuverable, and efficient flying robots can navigate complex environments. By understanding and replicating dragonfly-like flight, MAVs could achieve better stability, energy efficiency, and control in turbulent spaces. However, there remains a significant gap in aerodynamic research, with limited studies exploring the aerodynamic effects of biologically inspired corrugated wing structures, such as those of dragonflies, in dynamic, flapping motion. This lack of exploration into realistic wing geometries and dynamic flapping behaviors limits our understanding of how these structural adaptations influence aerodynamic forces like lift and drag. Investigating these effects is essential for accurately replicating dragonfly-like flight characteristics and harnessing their potential for bio-inspired air vehicle design. In this study, the objective is to investigate the aerodynamic effects of a 3D flapping dragonfly wing using computational fluid dynamics (CFD) in OpenFOAM. This is done through first adapting a static simulation to a 3D dynamic flapping model by employing dynamic meshing and Arbitrary Mesh Interface (AMI) to improve the accuracy of the simulation. In this way, this study is able to analyze how corrugated wing geometry influences flow characteristics, lift, and drag forces.

III. Background

A. Flight Mechanics and Agility of Dragonflies

Dragonflies exhibit a variety of flight behaviors that are achieved through unique mechanical adaptations, making them the subjects of intense study for biomimetic applications in MAV design. One of the most distinctive aspects of their flight capability is their wing structure and the corresponding kinematics. Dragonflies are capable of independent wing manipulation, allowing them to alter the stroke plane, α , and wing twist of each wing beat [1], but typically exhibit anti-phase flapping patterns in order to stabilize flight where the stroke of the forewings are coupled with the counterstroke of hind wings at a 180° phase difference [2]. This level of control enables behaviors such as rapid darting flights, precision hovering, and backward flying [3].

The agility of dragonflies is largely due to their ability to execute rapid wing motions [4], they achieve high power-to-weight ratios [5–7], faster speeds, and lower wingbeat frequencies compared to other flying insects; species of the genus *Orthetrum* have been observed with flapping frequencies in several works of literature, typically between 20-50 Hz [8–11], effectively reducing energy expenditure for maximum efficiency. Furthermore, their wings not only flap across but can also rotate, allowing for control of the flight vector both horizontally and vertically. This rotational movement is critical for making quick turns and sudden stops. These wings also operate aerodynamically under unsteady conditions where leading-edge vortices play a crucial role in lift generation. These vortices remain attached over a range of attack angles due to the corrugation of their wings, enhancing both lift and thrust during flapping flight. Lastly, the structural corrugation of dragonfly wings contributes to their aerodynamic efficiency by providing mechanical strength without a significant increase in weight, which is critical to the dynamic changes in flight speed and direction [12].

The integration of these biological insights into MAV design could revolutionize the approach to constructing flight systems for small-scale aircraft, especially in tasks that demand high maneuverability and efficiency in complex environments. By studying and replicating these natural flight mechanisms, researchers aim to enhance the performance of MAVs beyond the current capabilities of conventional airfoil-based designs.

B. Highly Corrugated Wing Structural Analysis

Dragonfly wings are distinguished by their corrugated morphology, and high aspect ratio (AR), which significantly enhance aerodynamic and structural efficiencies. Corrugated wing surfaces can lead to a reduction in drag by as much as 15% and an increase in lift by up to 20% in comparison to flat wings. These preferable aerodynamic forces are attributes of wing corrugation interactions with airflow [13]. Corrugations also increase the wing's torsional stiffness, making them more resistant to bending and twisting under load. This mechanical property is essential for the rapid wing flapping required for the diverse flight behaviors of dragonflies, such as quick turns and sudden stops. Research into the material properties of these wings reveals that the biologically inspired design principles employed can provide

significant insights for MAV technologies, where durability and flexibility are critical [14, 15]. By incorporating designs that emulate the natural corrugation of dragonfly wings, engineers can significantly enhance the structural robustness and aerodynamic efficiency of MAVs. This biomimetic approach not only aids in achieving greater agility and energy efficiency, but also opens new pathways for the development of MAVs capable of operating in more complex and turbulent environments.

C. Static Wing Gliding Flight Analysis

Various analyses of gliding flight investigate the aerodynamics of dragonfly wings in fixed-wing positions during non-flapping phases. Gliding flight becomes significant as an adaptation of thermoregulation to control temperatures raised by vibrations and flapping [16], and becomes particularly important when considering MAV design. Using several different techniques, researchers have determined how the physical characteristics of dragonfly wings, specifically their corrugated profiles, affect lift and drag. Studies reveal that dragonfly wings, even without flapping, generate significant lift to support extended glide phases due to the optimized structure that stabilizes airflow and minimizes energy loss during flight [14, 15, 17, 18].

One key finding is that the wing corrugation aids in maintaining continuous airflow over the wing. The complexity of the wing surfaces allows for generation of vortices within its geometric cavities, preventing flow separation as well as stall, allowing dragonflies to glide efficiently even at lower speeds [17]. CFD simulations correlate these observations with quantitative data, showing a direct relationship between wing morphology and aerodynamic performance. This is evident in how modifications to the wing's corrugation depth and frequency alter lift and drag coefficients, providing insights into the functional advantages of these structural features [14]. Further, by comparing the CFD results with flight data, researchers have validated and improved the accuracy of models of aerodynamic forces.

D. Dynamic Wing Flapping Flight Analysis

The dynamics of flapping flight have been investigated in many works with findings that interactions between the fore and hind wings are responsible for reduced lift values. It is significant to understand the evolutionary benefits of these dragonfly flight characteristics, such as increased efficiency as well as energy recovery. The work of Usherwood and Lehmann [19] concludes that the wing phasing can be optimized such that the hind wing captures the wake of trailing edge vortices generated by the fore wing. Optimal thrust generation phasing was proven to occur when a leading hind wing stroked with a 25% phase shift, which could greatly decrease power consumption [20].

These findings suggest that dragonflies have evolved independent wing control not only for aerodynamic efficiency but also for maneuverability and adaptability in different flight scenarios. Understanding these mechanisms provides valuable insights into both evolutionary biology and bio-inspired design. In our investigation using AMI dynamic meshing techniques, we explore the application of single-dimension dynamics of a rigid *Orthetrum caledonicum* wing, particularly as an initial step in replicating biological flight for the development of energy-efficient MAVs capable of sustained and agile flight.

IV. Methods

A. Initial and Boundary Condition Files

This section details the preparation of the necessary simulation files, all of which are *italicized* in the text, for the 3D dragonfly wing analysis. While other sections will focus on the relevant processes for the geometry and mesh generation, this section features the files for the boundary conditions, physical properties, system files, and solver settings required to execute the simulation. The preparation of these files involved selecting the appropriate turbulence model, defining the necessary boundary conditions, and adjusting the solver parameters, all of which were influenced by a comparison of different file types for a variety of simulation scenarios. The key challenge in this process was the shift in complexity from previously written files for a 2D static airfoil simulation. The setup for the 3D dragonfly wing simulation differs vastly, requiring detailed adjustments to account for the dynamic mesh motion and/or unsteady flow conditions and the additional complexity of three-dimensional aerodynamic effects.

First, the boundary condition and initial condition files were created. For the initial conditions, the initial velocity, pressure, and turbulence conditions were based on estimated flow parameters, and set in a way to ensure that all motion would be induced by the wing. The *k* file, which simulates turbulent kinetic energy, included values calculated from estimated turbulence intensity and mean flow velocity, ensuring consistency with the turbulence model that will be

specified in the *turbulenceProperties* file. We used cyclicAMI to allow for periodic interaction at sliding mesh interfaces, and the wing, front, back, and topAndBottom wall boundaries utilized the kqRWallFunction, to model the near-wall turbulence accurately. Finally, the inlet used turbulentIntensityKineticEnergyInlet, which used intensity of 0.05 to define realistic inflow turbulence and the outlet used zeroGradient to allow turbulence to exit naturally without artificial constraints. This setup ensured realistic turbulence modeling, proper wall treatment, and smooth mesh interactions for the dynamic flapping wing simulation.

The *nut* file, simulating eddy viscosity, also used values that were estimated using a combination of turbulence models and flow parameters, and matched the selected turbulence model. The usage of cyclicAMI maintained continuity at sliding mesh interfaces, and the nutkWallFunction for the boundary conditions properly modeled the near-wall turbulence effects. At the inlet, the calculated solver ensured smooth transition from internal field values, and at the outlet, zeroGradient allowed the turbulence viscosity to exit freely. This setup confirmed accurate near-wall turbulence modeling, smooth boundary transitions, and proper handling of the moving mesh interfaces for the flapping wing case.

The values in the *omega* file, which simulates specific turbulence dissipation rate, were derived based on turbulent kinetic energy and turbulence length scale, and used theoretical estimates to determine appropriate values. Once again, cyclicAMI ensured smooth transition at sliding mesh interfaces, omegaWallFunction properly modeled the near-wall turbulence dissipation, and using both turbulentMixingLengthFrequencyInlet for the inlet and zeroGradient for the outlet helped to define turbulence scale for realistic inflow conditions while allowing omega to exit freely at the end. This setup ensured accurate near-wall turbulence dissipation, smooth inflow conditions, and compatibility with the moving mesh dynamics, making it well-suited for the 3D flapping wing case.

The initial pressure file *p* sets the pressure boundary conditions to match the physical expectations of the simulation. Thus, the boundary conditions and inlet were set to fixedFluxPressure in order to maintain the correct pressure gradients while allowing for dynamic mesh adjustments, while the outlet remained at a fixedValue of 0 to provide a reference pressure to stabilize the solver. This setup allowed for smooth pressure distribution across the moving mesh, prevented artificial pressure buildup, and maintained realistic flow behavior for the 3D flapping wing case.

Finally, the initial velocity file *U* served a similar purpose, to define the initial and boundary velocity fields based on expected aerodynamic conditions, adjusted for inflow, outflow, and no-slip conditions at solid surfaces. The movingWallVelocity accurately captured wing motion effects on surrounding flow, and the fixedValue of (0 0 -0.1) for the inlet set a controlled inflow velocity for the simulation. The pressureInletOutletVelocity allowed for flow to exit naturally out of the outlet, while the noSlip condition on the other boundaries ensured realistic boundary layer formation on stationary surfaces. Throughout this setup of initial conditions, the simulation could be assured to showcase accurate wing motion effects, smooth velocity transitions, and proper inflow/outflow conditions for the wing simulation.

Initial/Boundary Condition	Value
<i>k</i>	0.00341
<i>nut</i>	0.00001
<i>omega</i>	0.10000
<i>p</i>	0.00000
<i>U</i>	0.00000
<i>nu</i>	0.00001

After this process, the physical property and material files were created. For the *transportProperties* file, the kinematic viscosity and density was defined based on air properties at the given simulation conditions, and this ensured consistency with experimental or reference values. The simulation utilized a Newtonian transportModel, as air behaves as a Newtonian fluid. Thus, the nu value represented the true kinematic viscosity of air (1e-05), making it appropriate for simulating aerodynamic effects at the *Re* relevant to dragonfly flight. As for the *turbulenceProperties* file, the purpose was to select an appropriate turbulence model and to verify that the model settings aligned with OpenFOAM's best practices for aerodynamic simulations. Therefore, the turbulence model chosen was the RASModel kOmegaSST, as this model captures turbulence near surfaces in free-stream, improving accuracy for complex aerodynamic flows like dragonfly wings. Turbulence was set to 'on' to enable turbulence modeling, in order to account for the unsteady aerodynamic effects relevant to flapping flight.

When it comes to the mesh and dynamic settings, such as the *dynamicMeshDict* file, this will be discussed in its own section at a later point in the paper. The next step was to create the relevant system files, such as the control and solver settings. The first of these files was the *controlDict* file, which set the simulation time step, write intervals, and runtime control settings. This file served to ensure a proper balance between accuracy and computational efficiency. Our

simulation utilized `pimpleFoam`, as it is suitable for transient turbulent flows with moving boundaries. We ensured small time steps ($dt = 0.0002$ s) to capture rapid wing motion while adjusting adaptively, and also made sure the simulation was kept numerically stable by controlling the Courant number. These settings ensure high temporal resolution, numerical stability, and efficient data storage, making them ideal for capturing the unsteady aerodynamics of flapping wings. The `decomposeParDict` file was created to configure domain decomposition for parallel processing, and to adjust the processor distribution based on available computational resources. For the method, the Scotch decomposition method was used as it automatically partitions the mesh into 8 subdomains to minimize the inter-processor communication, which would help with improving the load balancing for complex 3D geometries like the flapping dragonfly wing.

The last of the files to initially create were the numerical scheme and solver settings, with many of these settings already matching the parameters required for the dragonfly simulation through its usage in the 2D `wing_motion` case in OpenFOAM. The first of these files, `fvSchemes`, defined discretization schemes for gradient, divergence, and Laplacian terms. These settings ensure stability and accuracy by selecting the appropriate schemes. The Euler time scheme is stable for transient simulations of flapping motion, and the Gauss linear gradient scheme ensures accurate pressure and velocity gradients in 3D unsteady flow. The Laplacian scheme (Gauss linear limited correct 0.5) serves to handle the diffusion with non-orthogonal mesh corrections, and the surface normal gradient scheme being set to corrected; improves the accuracy in non-orthogonal meshes near wing surfaces. Finally, the `meshWave` setting for the wall distance calculation works well with the `k-omega SST` turbulence model chosen previously. Lastly, the `fvSolution` file served to configure the solver settings for pressure-velocity coupling, such as PIMPLE. This file also sets convergence criteria and relaxation factors for numerical stability. In creating this file, we used the GAMG solver for efficiency, a tight tolerance ($1e-7$) for accuracy, and chose the GaussSeidel smoother for stability in the simulation. Many other settings were pre-defined through referring to the 2D `wing_motion` case file, and were applicable to the current simulation as well, enabling the creation of the file to run smoothly. A final schematic of the grid, wing, and boundary condition types can be seen in Fig. 1.

This process of defining and refining the necessary files for the simulation ensured that all physical properties, boundary conditions, and solver settings were appropriately configured, providing a structured foundation for accurately modeling the aerodynamic behavior of the dragonfly wing.

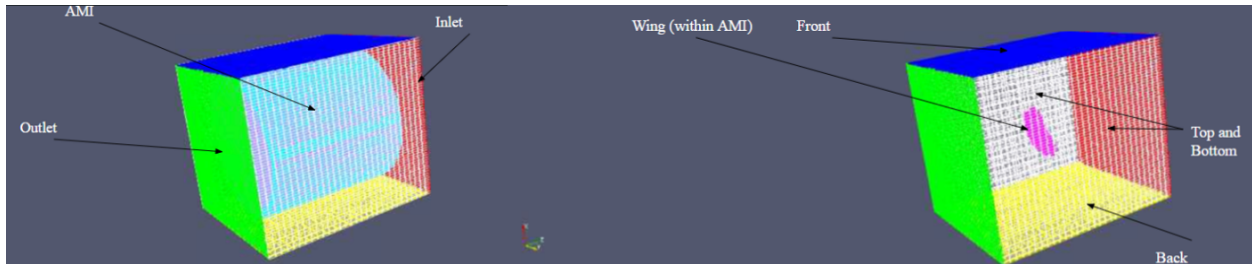


Fig. 1 Boundary Conditions

B. Static Case Meshing

For the static case, some changes were made to the initial condition and boundary files. The static analysis of the dragonfly wing utilizes the `simpleFoam` solver in OpenFOAM, which is well-suited for steady-state incompressible flow simulation. Unlike the `pimpleFoam` solver used for the dynamic case, `simpleFoam` allows for faster convergence while maintaining accuracy in capturing the aerodynamic forces acting on the stationary wing. Since the wing remains fixed in this study and does not create turbulence, unsteady effects are not important, making `simpleFoam` an appropriate choice. The case files for the static dragonfly simulation were adapted from the OpenFOAM motorbike tutorial, changing boundary conditions and mesh objects and bounds to be applicable to wing simulations. A zero pressure gradient was defined for the inlet and wall patches, while a reference pressure of 0 was defined at the outlet. The main driving condition for the simulation was the incoming velocity in the inlet patch and the internal field.

The computational mesh was generated using the `surfaceFeatureExtract` and `snappyHexMesh` commands. The dragonfly wing geometry was exported as an ASCII stl file. Before meshing, the geometry was translated to align with the origin of the computational domain to ensure that the wing was within the bounds of `blockMesh`. To capture the flow field accurately, a structured background mesh was created using `blockMesh`, defining a domain with dimensions of 1,400 cells in height, 1000 cells in width, and 1,600 cells in length. This domain size ensures that the flow has sufficient

space to develop around the wing and minimizes adverse wall effects. Unlike the dynamic simulation, no AMI was required, as the wing remains stationary. Thus, the surface feature extract only obtained the eMesh of a wing stl. This resulted in the snappyHexMesh locally refining only the wing region. The resulting mesh included a front, back, inlet, outlet, topAndBottom, and wing patches.

Aerodynamic performance was evaluated by computing C_L and C_D . A force coefficient function was implemented to normalize the forces acting on the wing patch. This function accounts for characteristic wing span of 800 mm, reference wing area of 160000 mm^2 , and free stream velocity magnitude of 5 m/s. These normalized values provide a dimensionless measure of the aerodynamics of the dragonfly wing, facilitating comparison across different angles of attack (AoA). To model realistic flight conditions, the simulation assumed a dragonfly cruise speed of 5 m/s, corresponding to a Re of 5000. The Re was maintained using the characteristic wing length and kinematic viscosity, ensuring that the flow regime matched typical dragonfly glide. The aerodynamic performance of the wing was analyzed across a range of AoAs, from 0° to 60° in 2° increments, to capture the full lift curve. Since simpleFoam solves for steady-state conditions, each AoA was treated as an independent simulation. Originally, the velocity vector in the 0 time directory was adjusted for each case to account for the AoA, with components defined as: $V_z=5\cos(\alpha)$, $V_y=-5\sin(\alpha)$. This approach produced concerning drag curves and failed to accurately model the AoA with incoming flow. To gain a more accurate simulation of the wing, OpenFOAM's surfaceTransformPoints command was used to rotate the geometry and snappyHexMesh was re-run for each AoA.

C. Dynamic Case Meshing

For the dynamic case, the computational mesh was created similarly to the static case but used two stls: the wing and the AMI, a surrounding cylinder aligned with the wing's rotation axis. The same surfaceFeatureExtract command was used to create an eMesh of the wing and cylinder surface. The blockMesh file created a domain surrounding the wing and AMI, where the inlet, outlet, front, back, topAndBottom, and wing patches were specified. The 3D mesh could then be generated with snappyHexMesh and renumberMesh. In order for the AMI surfaces to be treated as separate boundaries, createPatch specified the inside and outside surface of the cylinder as individual patches defined as cyclicAMI. This way, refinement along the rotating surface would increase the accuracy around the shifting mesh.

As for analyzing aerodynamic performance, the C_L and C_D values were calculated at each time step. The AoA did not change, as there was only flapping motion and no pitching motion. Instead, β changed throughout the simulation, which was the angle between the span of the wing and the x-axis, or initial position of the wing. To model realistic flight conditions, the AMI rotated between negative and positive 15 degrees, so A was set to 0.262 radians. The frequency of these flap cycles was set to 30 Hz, or 0.033 seconds per flap cycle.

V. Results

A. Static Case Results



Fig. 2 Wing Top Pressure Distribution



Fig. 3 Wing Bottom Pressure Distribution



Fig. 4 Front Pressure Graphic



Fig. 5 Dragonfly Wing Profile

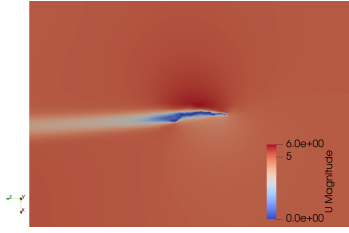


Fig. 6 Velocity Contour at Wing Center

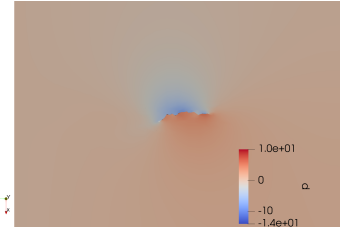


Fig. 7 Pressure Contour at Wing Center

The profile of the analyzed wing is pictured in detail in Fig. 5. The pressure and velocity distributions from different viewpoints are captured by Fig. 2, 3, 4, 6, and 7. These plots provide information about the behavior of the wing in a flow. Figures 4 and 7 support the fact that the wing must produce lift as there is a pressure gradient along the wing. The top of the wing consistently has a pressure value 1 Pa greater than the equilibrium value, while the bottom of the wing generally has a pressure value 1.4 Pa lower than the equilibrium value. In total, the pressure difference is 2.4 Pa. These values are confirmed by Fig 2 and 3, which show that the pressure values stay nearly constant on the surfaces of the wing except for along the leading and trailing edges of the wing. Figure 6 provides more insight into the velocity of the flow around the wing. It is in a free stream velocity of 5 m/s, but flow stagnates at the leading edge, speeds up to 6 m/s above the wing, and slows to around 3-4 m/s below the wing.

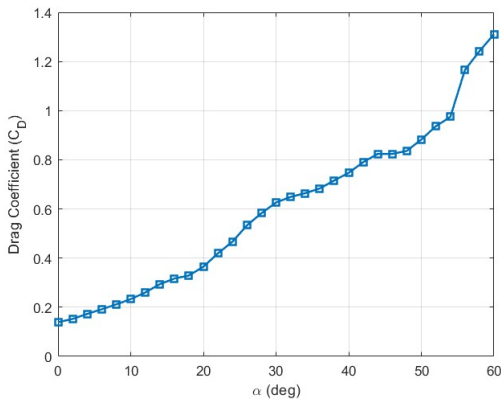


Fig. 8 C_D vs. α

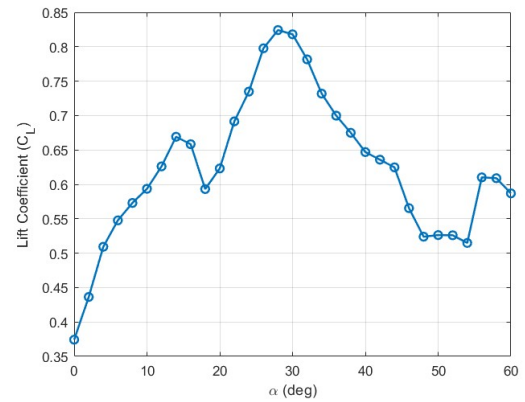


Fig. 9 C_L vs. α

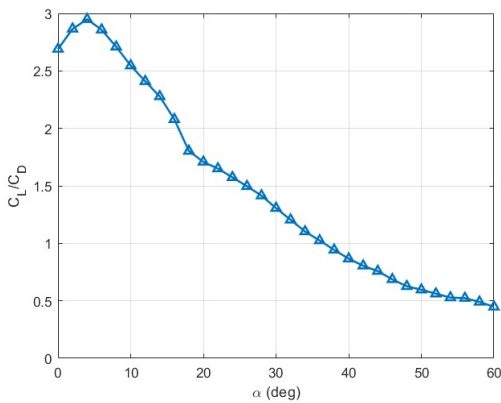


Fig. 10 C_L/C_D vs. α

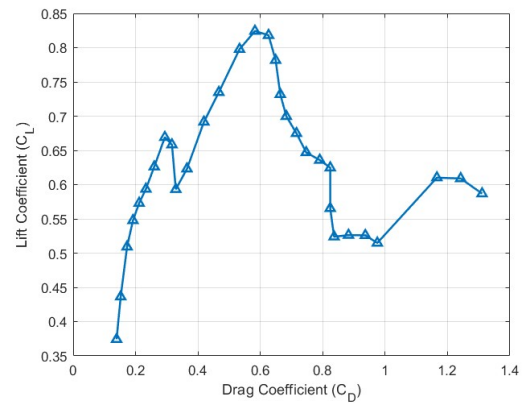


Fig. 11 C_L vs C_D

To analyze the aerodynamic performance of the dragonfly wing, the results from the simulation of the wing at each α were consolidated into four plots. One comparing the C_L to α , a second comparing the C_D to α , and two more

comparing the C_D to the C_L at each α .

Figure 8 summarizes the change in the C_D over the specified range of α . It is observed that at lower α between 0 and 50 degrees, the C_D increases gradually from 0.144 to 0.883. Following 50 degrees α C_D starts to rise sharply. The C_D of the dragonfly wing performs in a similar manner to standard aircraft wing geometries. On the other hand, Fig. 9 displays the nature of the relationship between α and C_L . The lift coefficient increases steadily until it reaches the first peak value of 0.669 at 14° . The C_L continues to increase until a maximum of 0.824 at 28° and declines past the stall point. Beyond the stall angle, the C_L decreases sharply, indicating the instability of the wing under higher α conditions. The C_L has a spike in increase at 56° but returns to its declining stall pattern. Figure 10 compares the C_L to the C_D at each respective AoA, providing information about the optimal operating conditions for the dragonfly wing chosen. The positive increase in the C_L to C_D ratio for low α values of 2° , 4° , and 6° indicates that lift is produced efficiently, with the best ratio of 3 at 6° . Beyond the peak α value, the negative slope of the curve indicates a higher amount of induced drag for the generated amount of lift, which can hinder the performance of the wing. The low angles of attack producing the higher C_L/C_D corroborates observations on the necessity of the dragonfly flapping mechanism to produce more lift without relying on AoA variation with drag consequences. The C_L vs. C_D plot in Fig. 11 looks similar to Fig. 8 because of the mostly linear increase of C_D with α .

B. Dynamic Case Results

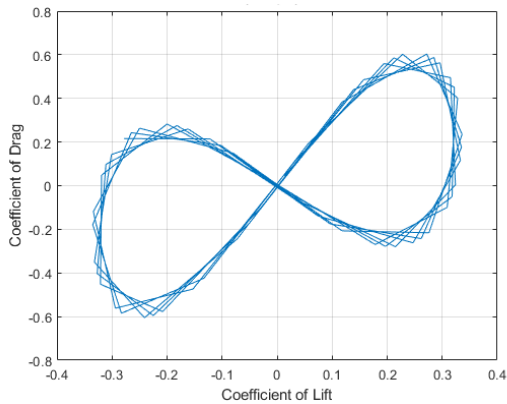


Fig. 12 C_D vs. C_L for Flapping Wing

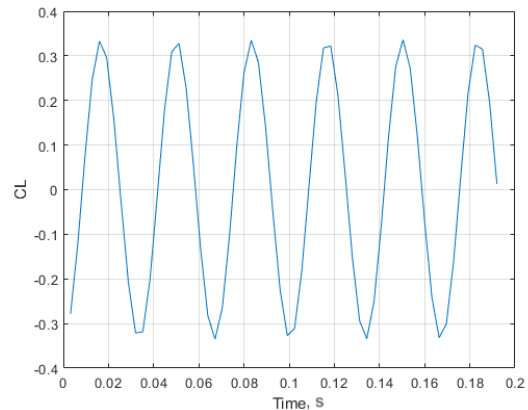


Fig. 13 C_L vs. Time for Flapping Wing

To analyze the flapping wing performance, two main graphs were created. Figure 12 is the C_L vs C_D graph at each time step, and Fig. 13 is a C_L vs time graph.

Figure 12 compares the C_L to the C_D at each time step, giving insight to how these values vary together as the wing angle changes. As the C_L increases from -0.1 to 0.1, the C_D increases linearly as well, however, this graph shows a general periodic trend where the C_L moves in an upward and downward pattern based on the looping motion of C_L vs C_D . For most of the graph, the C_L vs C_D generally repeats the same pattern of motion after the completion of each loop. The C_D reaches its maximum value of 0.6 when the C_L is roughly 0.23 and 0.27. The C_D reaches its minimum value of -0.6 when C_L is roughly -0.23. Figure 13 plots the C_L over time for the wing which gives insight into how these C_L values vary during flapping. As seen in the graph, there is a general sinusoidal curve present throughout the entire graph with a maximum C_L value of 0.34 occurring in iterations of 0.033 seconds starting at roughly 0.017 seconds and progressing with this iteration value until 0.192 seconds. The minimum C_L value in this graph is -0.34 which occurs at the same iterations starting at 0.033 seconds and progressing with this iteration value until 0.164 seconds.

Figure 14 shows the velocity distribution of the dragonfly wing at a time step of 0.0032 seconds. This figure provides insight into how different sections of the wing are more prone to higher velocity interactions than others. As seen in Fig. 14, the center of the wing experiences a magnitude of almost 0 m/s. As the wing expands in both directions outward from the center, the wing experiences higher velocities and hits a peak near the ends of the wing. In the streamline plot in Fig. 17, it is clear that there is a greater amount of activity occurring near the tip of the wing with the velocity vectors pointing radially outward and curving down toward the other end of the wing from left to right.

Figure 15 shows the velocity distribution of the dragonfly wing at a time step of 0.0512 seconds. In this image, the wing is experiencing higher velocities than the wing in Fig. 14. The center is experiencing roughly 0 m/s of velocities.



Fig. 14 Velocity Distribution at 0.0032s



Fig. 15 Velocity Distribution at 0.0512s



Fig. 16 Velocity Distribution at 0.192s

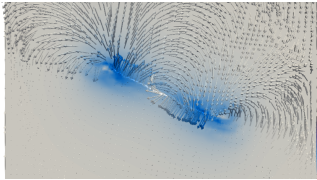


Fig. 17 Streamline Plot at 0.0032s

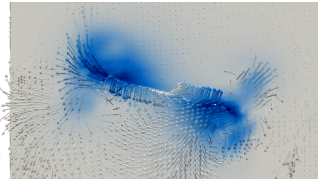


Fig. 18 Streamline Plot at 0.0512s

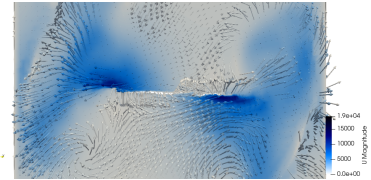


Fig. 19 Streamline Plot at 0.192s

However, as the wing extends past the center and near the tips, the velocities the wing experiences become greater. In the streamline plot in Figure 18, the peak velocity is seen concentrated near the tips of the wing with the velocity vectors extending out of the left end of the wing and extending into the right tip of the wing.

Figure 16 shows the velocity distribution of the dragonfly wing at a time step of 0.192 seconds. In this image, the wing experiences only velocities of roughly 0 m/s throughout the entire wing and does not have concentrations of peak velocities unlike Fig. 14 and Fig. 15. However, the streamline plot, Figure 19, corresponding to this figure shows concentrations of velocities much greater than 0 m/s near the tips of the wing.

VI. Discussion

A. Static Case Discussion

The static case reveals much about the aerodynamic efficiency of the dragonfly wing under glide conditions. The plots described above can be analyzed considering the geometry of the wing as well as their deviations from typical airfoil behavior.

As shown in Fig. 8, the C_D vs AoA plot increases throughout the whole range of angles selected and particularly after an α of 50° . This behavior is expected as the C_D typically increases with α as a result of increased flow separation, especially at fairly high AoAs.

Furthermore, Fig. 9 affirms that the dragonfly wing behaves according to the typical trend between the C_L and AoA observed in many standard airfoils where the C_L steadily rises until the stall angle, at which point high amounts of flow separation prevents the production of lift and leads to sharp drop in the C_L value. However, the stall angle for the dragonfly wing is 30° which proves to be significantly higher than the typical stall angle for smooth airfoils at about 15° . The ability for the dragonfly wing to produce lift at higher AoAs than usual is likely due to the corrugated nature of its geometry. The corrugation allows for the flow to remain continuous and for the leading edge vortices to remain attached for a longer duration. Flow is able to pass more easily over the wing as the ridges in the wing provide “paths” and act as “guides” for the flow. In addition, Fig. 2, 3, 4, and 7 supports the fact that the wing is able to produce lift because of the pressure gradient along the wing. The pressure on the bottom of the wing is higher than the pressure on the top of the wing. This observation aligns with typical airfoil behavior and the reasoning behind the generation of upward lift in an airfoil.

Observing the relationship between the C_L and C_D proves to be important when considering the applications of corrugated airfoil structure to airfoil design. The optimal operating condition for the dragonfly wing according to Fig. 10 is achieved at an α of 6° . It is important to analyze this limitation and develop strategies to ensure that operating conditions remain below this value so that any advancements made incorporating bio-inspired technology are still safe for use. While these findings are useful in observing and quantifying the behavior of a dragonfly wing and their efficiency when under a gliding mode of flight, these results are based on idealized computational simulations. Further, real-world testing in a wind tunnel or more advanced modeling assuming varying Re , compressible flow, or unsteady

flow would be beneficial to gather more specific insights.

B. Dynamic Case Discussion

The dynamic case aims to improve our understanding of the aerodynamics that result from the flapping motion of the dragonfly wing. The plots above can be analyzed considering the type of motion as well as the geometry of the wing. As shown in Fig. 12, the values for C_L and C_D respective for each time step increase and decrease according to the instantaneous position of the wing during its full motion. The asymmetry of the plot could be further explored by observing any differences in the efficiency of one stroke over the other. There are periods where lift is generated in the upward direction by the downstroke of the flap and the opposite occurs during the upstroke of the flap. The portion of the loop where lift increases represents the downstroke and the portion of the loops where lift is decreasing represents the upstroke. The relatively large changes in C_D where C_L is at its minimum and maximum represents the high amounts of drag generated for the respective amount of lift. It represents the points in the motion at which the direction of drag generation flips. Similarly, where the loop intersects is where the direction of drag and lift generation flips. The high amounts of drag is likely due to vortices or unsteady wakes of the flow.

This is further supported by Fig. 14, 15, and 16, which display the velocity distribution along the wing at varying time steps. In Fig. 14 and 15 there is a gradient in the velocity along the wing. There are areas of higher velocities at the tips of the wing indicating more disturbance in the flow in these areas, and likely the cause of high drag. The higher velocities at the tips of the wing is due to the unsteady flow visible in the streamline plots Fig. 17 and 18. In contrast, Fig. 19 corresponds to a time step where the wing is at an equilibrium position and displays minimal unsteady flow, corresponding to the point at which lift and drag production changes direction. Figure 14 supports this characteristic with the absence of a velocity gradient along the wing.

As shown in Fig. 13, the values for C_L and the time progression of the flapping wing act in a predictable sinusoidal pattern which gives insights into the optimal times to maximize and minimize C_L for this specific dragonfly wing. There is a 0.68 change in C_L from its lowest value to its highest value indicating which time steps can be traced back to determine an optimal C_L for certain wing configurations. Further observations could be garnered by experimenting with different Re , or the wings of other species of dragonflies.

VII. Conclusion

The results of this study demonstrate that the flapping motion of the dragonfly wing generates complex flow patterns, influencing aerodynamic performance. The corrugated wing geometry plays a crucial role in enhancing lift, decreasing drag, and controlling airflow. The usage of dynamic meshing in OpenFOAM preserves mesh quality during motion simulations, serving to validate its effectiveness for bio-inspired flight analysis. Ultimately, understanding dragonfly wing aerodynamics can help to refine fluid-structure interaction models for real-world wing behavior in the future, guiding the optimization of wing shapes to improve aerodynamic efficiency in MAVs. These findings provide quantitative insights into lift and drag across multiple flapping cycles. The results in this study can help to inform future research directions, such as through incorporating flexible wing models to study their influence on aerodynamics, further refining turbulence modeling and boundary conditions for increased simulation accuracy, and working to ultimately expand the analysis to include multi-wing interactions to explore the realistic way in which dragonflies coordinate their forewings and hindwings for enhanced flight control. These findings can be applied to developed advanced MAV designs, leveraging corrugated wing structures for improved lift, drag reduction, and energy efficiency, bringing aerospace applications one step closer to replicating the unparalleled aerodynamics of natural flyers.

Acknowledgments

We would like to thank Professor Suhas Jain and Luis Hatashita for their guidance throughout our VIP research process.

References

- [1] Zhu, S. B. X. D. Y. W. L. X. Y. X., Z., “Three-dimensional sweeping motion effects on hovering dragonflies,” *Aerospace Science and Technology*, Vol. 127, 2022. <https://doi.org/https://doi.org/10.1016/j.ast.2022.107701>.
- [2] Alexander, D., “Unusual Phase Relationships Between The Forewings And Hindwings In Flying Dragonflies,” *J Exp Biol*, Vol. 109, No. 1, 1984, p. 379–383. <https://doi.org/https://doi.org/10.1242/jeb.109.1.379>.
- [3] Bode-Oke, Z. S. D. H., A. T., “Flying in reverse: kinematics and aerodynamics of a dragonfly in backward free flight,” *Journal of the Royal Society Interface*, Vol. 15, No. 143, 2018. <https://doi.org/https://doi.org/10.1098/rsif.2018.0102>.
- [4] Büsse, G. C. H. T., S., “Homologization of the Flight Musculature of Zygoptera (Insecta: Odonata) and Neoptera (Insecta),” *PLOS ONE*, Vol. 8, 2013, pp. 1–16. <https://doi.org/https://doi.org/10.1371/journal.pone.0055787>.
- [5] Pan, G. S. W. J. H. X., Y., “Aerodynamic performance of a flyable flapping wing rotor with dragonfly-like flexible wings,” *Aerospace Science and Technology*, Vol. 148, 2024, p. 109090. <https://doi.org/https://doi.org/10.1016/j.ast.2024.109090>.
- [6] Wakeling, E. C. P., J. M., “Dragonfly Flight: III. Lift and Power Requirements,” *J Exp Biol*, Vol. 200, No. 3, 1997, p. 583–600. <https://doi.org/https://doi.org/10.1242/jeb.200.3.583>.
- [7] Salami E., M. E. G. N. N. N., Ward T.A., “A review of aerodynamic studies on dragonfly flight,” *Proceedings of the Institution of Mechanical Engineers, Part C: Journal of Mechanical Engineering Science*, Vol. 233, No. 18, 2019, pp. 6519–6537. <https://doi.org/https://doi.org/10.1177/0954406219861133>.
- [8] Sun, L. S. L., M., “A computational study of the aerodynamic forces and power requirements of dragonfly (*Aeschna juncea*) hovering,” *J Exp Biol*, Vol. 207, No. 11, 2004, pp. 1887–1901. <https://doi.org/https://doi.org/10.1242/jeb.00969>.
- [9] Yu, Z. H. X. R. S. Y. . W. K., W., “Characterization of Wingbeat Frequency of Different Taxa of Migratory Insects in Northeast Asia,” *Insects*, Vol. 13, No. 6, 2022. <https://doi.org/https://doi.org/10.3390/insects13060520>.
- [10] Sivasankaran, W. T. S. E. V. R. F. C. J. M., P.N., “An experimental study of elastic properties of dragonfly-like flapping wings for use in biomimetic micro air vehicles (BMAVs),” *Chinese Journal of Aeronautics*, Vol. 30, No. 6, 2017, pp. 726–737. <https://doi.org/https://doi.org/10.1016/j.cja.2017.02.011>.
- [11] Aracheloff, C., Garrouste, R., Nel, A., Godoy-Diana, R., and Thiria, B., “Subtle frequency matching reveals resonant phenomenon in the flight of Odonata,” *Journal of the Royal Society Interface*, Vol. 21, No. 219, 2024, p. 20240401. <https://doi.org/https://doi.org/10.1098/rsif.2024.0401>.
- [12] Sun, B. B., J., “The structure and mechanical properties of dragonfly wings and their role on flyability,” *Comptes Rendus Mécanique*, Vol. 340, No. 1-2, 2012, pp. 3–17. <https://doi.org/https://doi.org/10.1016/j.crme.2011.11.003>.
- [13] Jongerius, L. D., S.R., “Structural Analysis of a Dragonfly Wing,” *Exp Mech*, Vol. 50, 2010, p. 1323–1334. <https://doi.org/https://doi.org/10.1007/s11340-010-9411-x>.
- [14] Kesel, A., “Aerodynamic Characteristics of Dragonfly Wing Sections Compared with Technical Aerofoils,” *J Exp Biol*, Vol. 203, No. 20, 2000, p. 3125–3135. <https://doi.org/https://doi.org/10.1242/jeb.203.20.3125>.
- [15] Levy, S. A., D., “Parameter study of simplified dragonfly airfoil geometry at Reynolds number of 6000,” *Journal of Theoretical Biology*, Vol. 266, No. 4, 2010, pp. 691–702. <https://doi.org/https://doi.org/10.1016/j.jtbi.2010.07.016>.
- [16] May, M., “Thermoregulation and Adaptation to Temperature in Dragonflies (Odonata: Anisoptera),” *Journal of Bionic Engineering*, Vol. 46, 1976, pp. 1–32. <https://doi.org/https://doi.org/10.2307/1942392>.
- [17] Wakeling, E. C. P., J. M., “Dragonfly Flight: I. Gliding Flight and Steady-State Aerodynamic Forces,” *J Exp Biol*, Vol. 200, No. 3, 1997, p. 543–556. <https://doi.org/https://doi.org/10.1242/jeb.200.3.543>.
- [18] Benedetti, B. G. C. S. B. M., L., “A numerical study about the flight of the dragonfly: 2D gliding and 3D hovering regimes,” *International Journal of Engineering Research and Technology*, Vol. 13, No. 11, 2020, pp. 3310–3320. <https://doi.org/https://doi.org/10.37624/IJERT/13.11.2020.3310-3320>.
- [19] Usherwood J.R., L. F., “Phasing of dragonfly wings can improve aerodynamic efficiency by removing swirl.” *J R Soc Interface*, Vol. 5, No. 28, 2008, pp. 1303–1307–1307. <https://doi.org/https://doi.org/10.1098/rsif.2008.0124>.
- [20] Shilong, M. S., L., “Aerodynamic force and flow structures of two airfoils in flapping motions,” *Acta Mech Sinica*, Vol. 17, 2001, pp. 310–331. <https://doi.org/https://doi.org/10.1007/BF02487459>.